Evaluation of MRI-based radiomic features in heart morphologic variations as a consequence of autoimmune thyroid disorders

Oliver Barachini[a], Michaela Schaer[a], Siroos Mirzaei[b], Klaus Hergan[c], Shahin Zandieh[a,c,*]

Abstract

Radiomics (RC) was initially developed using computed tomography (CT) for oncological imaging. However, it can be applied to various scientific and clinical radiology fields regardless of the modalities involved. The purpose of this survey was to evaluate alterations in magnetic resonance imaging of the heart (CMR) in patients suffering from autoimmune thyroid disorders (AITD) by applying RC tools and mapping features. A total of 50 individuals were evaluated in this study. We searched for CMR examinations performed in our department between January 2019 and 2021 in patients with AITD. Thirty patients with AITD (21 men and 9 women, aged 51 to 78 years; mean age, 60 years) were enrolled in our survey. We enrolled a control group (CG) of 20 individuals (14 men and 6 women aged 53–87 years; mean age, 68 years) without AITD or cardiac disorders. Global native T1 and T2 mapping revealed no significant differences between groups. However, we identified significantly higher values of several texture parameters, including the gray-level co-occurrence matrix (GLCM) entropy, gray-level run-length matrix (GLRLM; short-run high gray-level emphasis (SRHGE), GLCM (Energy), gray-level size zone matrix length matrix (GLZLM; LZLGE), GLZLM (SZLGE), DISCRETIZED (HISTO-Energy) GLCM (Dissimilarity), and GLCM (Contrast), in patients with AITD in comparison to the CG ($P <$ .01). Our results indicate that several RC properties extracted from CMR images can be used to discriminate between the AITD and CG groups.

Abbreviations: AITDs = autoimmune thyroid disorders, BP = blood pressure, CAT = chronic autoimmune thyroiditis, CG = control group, CMR = cardiac magnetic resonance imaging, CO = cardiac output, DCM = dilated cardiomyopathy, ECG = electrocardiogram, EDV = end-diastolic volume, ESV = end-systolic volume, GD = Graves' disease, GLCM = gray-level co-occurrence matrix, GLDZM = gray-level distance zone matrix, GLRLM = gray-level run-length matrix, GLSZM = gray-level size zone matrix, GLZLM = gray-level zone length matrix, HR = heart rate, LVEF = left ventricular ejection fraction, RC = radiomics, TSH = thyroid-stimulating hormone.

Keywords: Radiomics, autoimmune thyroid disorders, cardiac magnetic resonance imaging, mapping

1. Introduction

In autoimmune thyroid disorders (AITDs), damage to thyroid cells and antibody-mediated autoimmune responses are the major indicators of prognosis.[1] The dysfunction of the thyroid gland influences the physiology of other organs. Additionally, the effect of thyroid hormones on the cardiac system is an obvious clinical manifestation of thyroid disorders. Hormonal imbalance of the thyroid affects heart rate (HR), myocardial oxygen absorption, heart muscle contractility, blood pressure

(BP), and cardiac output (CO).[2,3] Congestive heart failure, tachyarrhythmia, and valve dysfunction can be other effects of thyroid hormone imbalance.[4] Clinical studies have suggested that subclinical hypothyroidism may impair ventricular function.[5,6]

Overt or subclinical hyperthyroidism can lead to increased cardiovascular mortality, HR, and CO as described by Selmer et al.[7]

Magnetic resonance imaging of the heart (CMR) is currently the gold standard for myocardial tissue characterization. Over the past few years, mapping techniques for CMR imaging have become

[a] Department of Radiology and Nuclear Medicine, Hanusch-Hospital, Vienna, Austria, [b] Department of Nuclear Medicine with PET-center, Wilhelminenspital, Vienna, Austria, [c] Department of Radiology, Paracelsus Medical University of Salzburg, Austria.

*Correspondence: Shahin Zandieh, Department of Radiology and Nuclear Medicine, Hanusch-Hospital, Heinrich-Collin-Strasse 30, A-1140 Vienna, Austria (e-mail: zandieh.s@icloud.com).

Key points

Multiple RC features extracted from CMR images discriminate between the AITD group and CG.

Global native T1 and T2 mapping revealed no significant differences between the AITD and CG.

A significant negative correlation was found between fT3 level and ESV and EDV, and a significant positive correlation was found between fT3 level and LVEF in patients with AITD and DCM.

increasingly important. Four major tissue parameters have been widely used: T2 mapping, T1 mapping, T2* mapping, and calculation of extracellular volume. These techniques provide information regarding intracellular disturbances (e.g., iron overload), extracellular disturbances (e.g., fibrosis), or both (e.g., infarction). These mapping techniques enable both the quantification and visualization of the disorder's extent.[8] Furthermore, these techniques offer tissue characterization based on quantitative alterations that can be recognized on color-aided maps of the heart.[9] Moreover, radiomics (RC), which was initially developed from computed tomography (CT)-based oncological imaging,[10] can be applied to various areas of radiology, independent of the modality of choice. In addition, using RC, a large amount of information that cannot be registered by the human eye can lead to improved diagnostic accuracy. In this context, factors such as the density, time, shape, and degree of contrast enhancement can be used for evaluation purposes. This raises the question of whether RC techniques or mapping can be used to effectively incorporate information from medical imaging to make more accurate decisions.

This study aimed to evaluate alterations in the CMR of patients with AITD using RC and mapping features.

2. Methods

2.1. Patient selection

Data from 50 individuals were analyzed. We searched for cases of CMR performed from January 2019 to 2021 for patients with AITD. Thirty patients with AITD (21 men and 9 women aged 51–78 years; mean age, 60 years) were enrolled in our study. The individuals had a mean body mass index (BMI) of 27 and a mean weight of 86 kg. Two individuals with chronic autoimmune thyroiditis (CAT) underwent thyroxin substitution for no more than 2 months during imaging examinations. No medications were used by any of the other participants. A control group (CG) of 20 individuals (14 men and 6 women aged 53–87 years; mean age: 68 years) without AITD or heart disease were enrolled in the survey. The mean BMI of the participants in the CG was 25, and the mean weight was 79 kg. Individuals with diabetes mellitus, hereditary nonthyroidal heart affections, renal disorders, pituitary affection, and/or pregnancy were excluded. Subjects displayed no signs of drug, alcohol, or toxic substance addictions. Clinical examinations ruled out nutritional deficiencies. Negative human immunodeficiency virus and hepatitis C virus serologies eliminated potential viral causes. There was no history of fever, joint pain, chest pain and cough, loss of weight, or loss of appetite. In the CG, the subjects were healthy and without any identified cardiac disorders.

No inherited causes were detected in patients with dilated cardiomyopathy (DCM). The CG consisted of healthy individuals without any detected heart disorder.

The patients were diagnosed with DCM based on chest radiographs, laboratory tests, echocardiography, electrocardiography (ECG), and CMR examinations. Atrial fibrillation was detected using electrocardiography. CMR was performed based on the ambiguous findings of the echocardiography survey.

All patients with AITD were diagnosed with Graves' disease (GD) or CAT. The CAT diagnosis was based on the presence of diffuse heterogeneity or hypoechogenicity of the thyroid tissue on sonography and the identification of high antiTG or antiTPO titers in the blood samples. GD was diagnosed using the American Thyroid Association criteria. Initial diagnoses of thyrotoxicosis were confirmed based on the presence of antibodies against TSH receptors and suppression of thyroid-stimulating hormone (TSH).[11]

2.2. Echocardiography

Echocardiography was performed by an experienced cardiologist using a Vivid 9 scanner with a 3.5 MHz transducer in the second harmonic mode (GE Vingmed, Horten, Norway). First, we performed a standard echo test to identify the dimensions. The data were obtained from standard chamber views. The Simpson biplane method was used to compute left ventricular ejection fraction (LVEF) and volume.

2.3. CMR

CMR imaging was conducted on all 50 individuals using a 1.5 T scanner (Magnetom, Siemens Medical Systems, Munich, Germany). Standard software for ECG-triggered image acquisition and phased-array coil were used in the survey.

In our study, true fast imaging with steady-state precession (FISP) and T2-weighted breath-hold sequences were used. Additionally, we acquired the vertical long-axis, short-axis, 4-chamber, and 5-chamber views. To detect regional wall motion alterations, we used true FISP sequences. The parameters utilized for true FISP cine imaging were temporal resolutions of 35 ms to 39 ms, a repetition time/echo time of 48.44/1.35 ms for all subjects, a 66° flip angle of 530, and an in-plane resolution of 1.4 mm² to 1.74 mm². A late gadolinium-enhanced sequence was applied 10 minutes after the intravenous administration of 0.5 mmol/kg gadoterate meglumine (Gd-DOTA; Guerbet, Paris, France) using an inversion recovery-prepared, T1-weighted gradient echo sequence.

2.4. Data analysis

Data postprocessing was performed using a commercially available workstation (syngo.via; Siemens Medical Systems, Munich, Germany).

Two experienced radiologists with more than 10 years of experience retrospectively analyzed the images. The patients' clinical histories and results were unknown to radiologists.

κ statistics were used for interobserver agreement assessment. A mean κ index (k) value of 0.76 for the CMR results was considered good.

The endocardial and epicardial contours of the left ventricle in the end-systolic and end-diastolic states were drawn by radiologists.

The contours were used to detect global parameters, such as end-systolic volume (ESV), end-diastolic volume (EDV), and left ventricular mass. Using the EDV and ESV parameters, secondary values, such as systolic volume (SV; EDV-ESV) and LVEF (LVEF = SV/EDV), were obtained for each subject.

The left ventricular diameter (LVD), left ventricular myocardial thickness, and ventricle were measured using CMR. LVEF regular values were based on surveys by Kawel-Boehm et al[12] and Plana et al[13] HR and BP values were identified throughout the CMR examination. CO measurement was based on ESV, EDV, and HR values.

2.5. Image preprocessing and radiomics

LIFEx software (version 6.3) was used for the implementation of RC.[14] The value of the region of interest (ROI) was 10 mm, which was placed in the septum in the T1-weighted sequence.
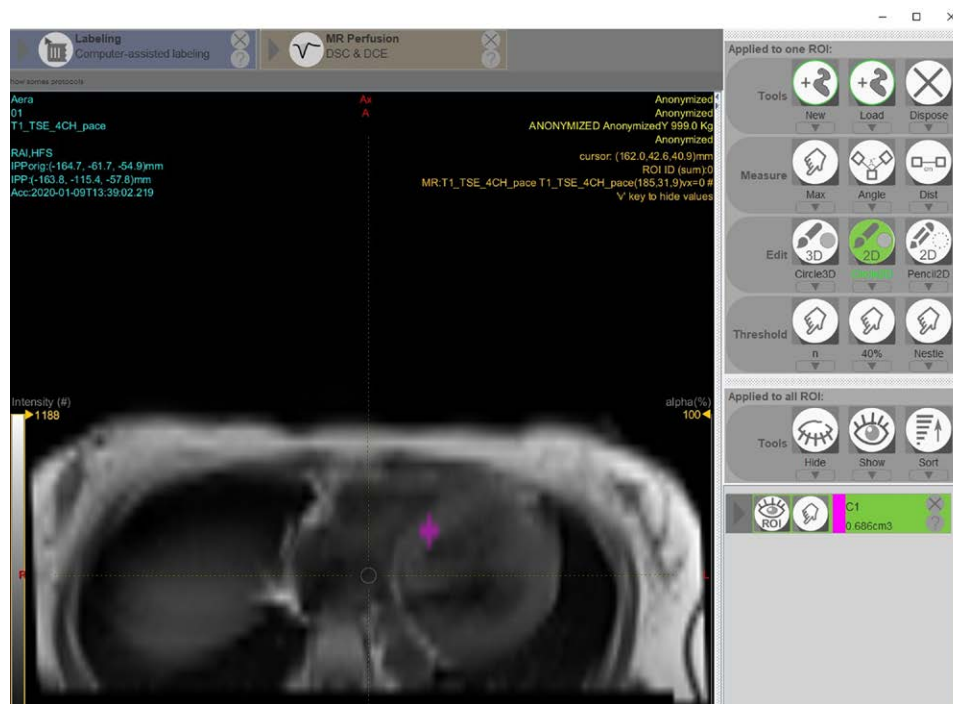
Figure 1. CMR 4-chamber view of the heart, analyzed by the LIFEx software user interface. The ROI of the septal wall has been used for radiomics feature computation.

The software extracted 36 texture parameters from the ROI and 31 second-order and 5 first-order parameters. The RC parameters and their explanations are described in the manual of the LIFEx software[14] (Fig. 1).

First-order parameters were based on single-voxel or single-pixel evaluations. These parameters were predicted by using gray-level histograms. The gray-level minimum, mean, maximum, variance, and percentiles are part of the first-order parameters.

Kurtosis and skewness were used to evaluate the shape of the intensity distributions and to obtain more elaborate properties. Skewness was used to evaluate data asymmetry. The distribution curve is reflected by skewness.

The tail of the data distribution is reflected by kurtosis because of outliers relative to a Gaussian distribution. Histograms of entropy and uniformity as well as other data characteristics were constructed.

In the current study, we calculated the following RC histogram and shape-based features: entropy (which characterizes the randomness of pixel distribution), skewness, sphericity (regularity of volume shape), kurtosis (peak of distribution), energy (homogeneity [closeness of voxel pairs] or uniformity of pixel distribution), and compacity (compactness of volume shape).

2.6. The gray-level co-occurrence matrix (GLCM) is the second-order gray-level histogram

Properties such as the spatial relationship between the pairs of pixels or voxels with predefined gray-level intensities in different directions and a predefined distance between pixels or voxels, such as energy, homogeneity, entropy, contrast, correlation (gray-level linear dependence), and dissimilarity (variation of the voxel pairs), were captured by GLCM. It also featured information about the neighborhood gray-level dependence matrix with coarseness, that is, the difference in the intensity between regions and contrast or the spatial rate change of intensity.[15] The gray-level run-length matrix (GLRLM), gray-level zone

length matrix (GLZLM), gray-level size zone matrix (GLSZM), and gray-level distance zone matrix (GLDZM) include information about the spatial distributions of runs regarding consecutive pixels with the same gray level or more directions and in 2 or 3 dimensions.[16]

In the GLSZM, information about the number of zones of interconnected neighboring pixels or voxels with the same gray level that form the basis for the matrix was included and calculated with a single co-occurrence matrix. Consecutively, information about the size of homogenous runs for each gray level was directly supplied in 3 dimensions.[17,18]

2.7. Statistical analysis

SPSS software (version 23; IBM) was used for statistical evaluation. Analysis of variance (ANOVA) was used to evaluate the differences between patient groups.

Bland and Altman plots were used to define the limits of agreement between imaging procedures, which were estimated as the mean difference (bias) and 2 standard deviations (SDs) of the differences (Fig. 2).

A 2-tailed test with P-values < 0.05 was used to determine the distinction between the standard echo measurements and MRI of VST, LVD, and LVEF.

3. Results

The present study included 50 participants: 30 patients with AITD and 20 healthy individuals. CAT was diagnosed in 16 (12 females and 4 males) of the 30 patients. In the CAT group, the thyroid volume was small in > 50% of the patients.

At the time of CMR, the mean serum TSH value of the CAT group was 6.2 mIU/L (range: 1–17 mIU/L). GD was diagnosed in all remaining patients. At the time of CMR, 2 females and 2 males with a mean serum TSH of 0.1 mIU/L (range: 0.01–0.3 mIU/L) were diagnosed with GD. In the CG, TSH values ranged from 0.3 mIU/L to 4.1 mIU/L. In addition, 7% of individuals with AITD and 60% of individuals with GD had cardiac palpitations.
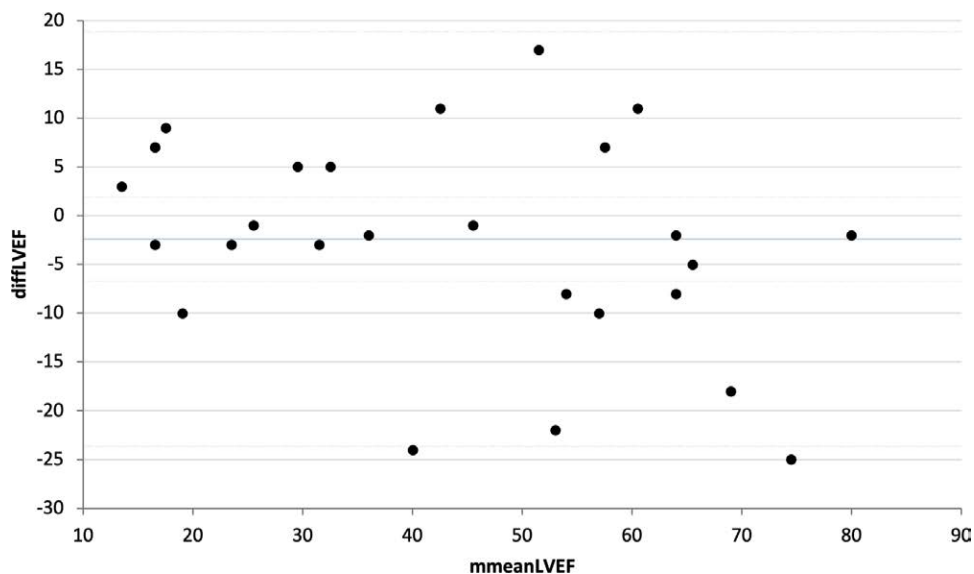
Figure 2. Bland-Altman plots were prepared to assess the agreement between echocardiography and CMR measures of LVEF. Bland-Altman diagrams of LVEF demonstrating mean differences and limits of agreement between baseline echocardiography and CMR findings.

Table 1

The mean CMR results of the AITD patients, and the CG are presented in the table.

	Mean TSH	EDV	ESV	SV	CI	LVEF	LVD	VST	MM
AITD	3.4 mIU/l	113.1 ± 45	65.5 ± 29	49.5 ± 23	2.7 ± 1	55.7 ± 10	5.5 ± 1	9 ± 3	90.2 ± 47
CG	2.2 mIU/l	132.8 ± 55	92.6 ± 47	63.8 ± 22	2.6 ± 1	68.5 ± 12	6,3 ± 1	10.7 ± 3	97.8 ± 29

AITD = autoimmune thyroid disorder, CI = cardiac index, CG = Control subjects, EDV = end-diastolic volume, ESV = end-systolic volume, LVEF = left ventricular ejection fraction, LVD = left ventricular diameter, LVMT = left ventricular myocardial thickness, MM = myocardial mass, SV = stroke volume, VST = ventricular septal thickness.

Four patients had DCM with a mean serum TSH of 7.4 mIU/L (range: 0.3–16.71 mIU/L) at the time of CMR inquiry. Toxic substance addiction and nutritional deficiencies were not detected. Hepatitis C virus and human immunodeficiency virus serology test results were negative. No clinical signs of chest pain, cough, joint pain, fever, appetite loss, or weight loss were observed. The 4 patients with DCM showed a reduced ejection fraction in the CMR, as shown in Table 1.

In patients with DCM, the LVEF was 40%. Three months after the CMR inquiry, echocardiography showed significant improvements in systolic LVEF. The mean value was 48% in DCM patients. In patients with both AITD and DCM, a significant negative correlation was detected between fT3 level and ESV ($R = 0.64$, $P < .002$) and EDV ($R = 0.63$, $P < .001$). A significant positive correlation was detected between fT3 level and LVEF ($R = 0.59$, $P < .001$). Furthermore, Pearson's correlation analysis demonstrated a significant positive correlation between TSH levels and ESV ($R = 0.57$, $P < .01$) and EDV ($R = 0.69$, $P < .01$) in patients with both AITD and DCM.

In patients with AITD, the mean EDV, ESV, and EF values were 160.2, 94.3 mL, and 45.2%, respectively. The CG showed a mean EDV, ESV, and EF of 111.2 mL, 37.7 mL, and 68.5%, respectively.

3.1. CMR was used for tissue characterization to rule out other diseases

No abnormalities were detected in the late gadolinium-enhanced or T2-weighted images. T1 and T2 mapping revealed no significant differences between the groups (Figs. 3 and 4). However, we found significant differences in the texture features GLCM (entropy), GLRLM (SRHGE), GLCM (Energy), GLZLMLZLGE,

GLZLM (SZLGE), DISCRETIZED (HISTO-Energy), GLCM (Dissimilarity), and GLCM (Contrast) between patients with AITD and CG ($P < .01$), as shown in Figures 5 and 6.

4. Discussion

Previous studies have shown that thyroid disorders can initiate severe cardiac dysfunction if the condition is not recognized in early stages. Even at the subclinical stage, AITD can lead to heart dysfunction.[19]

A few studies have reported cardiac dysfunction induced by thyroid disorders using CMR; these studies have shown significant changes in CI, CO, ESV, SI, and LVD between GD patients and controls. High reproducibility and accuracy are the key features of CMR as a method for evaluating functional and structural cardiac changes.

The impact of thyroid hormone on the cardiovascular system results in characteristic signs of thyroid disorder. Hypothyroidism and hyperthyroidism lead to changes in cardiac output, cardiac contractility, and myocardial oxygen consumption.

Thyroid hormone affects cardiac myocytes via expression of key structural and regulatory genes.[20,21]

Direct measurements of T1 and T2 times represent an alternative to conventional T2- and T1-weighted methods. The advantages of the direct measurement of T1 and T2 times compared to conventional techniques are that the former is a more sensitive quantification of myocardial T1 and T2 times, less susceptible to artifacts caused by movement and arrhythmias, and more objective as an examiner-independent form of evaluation.[22]

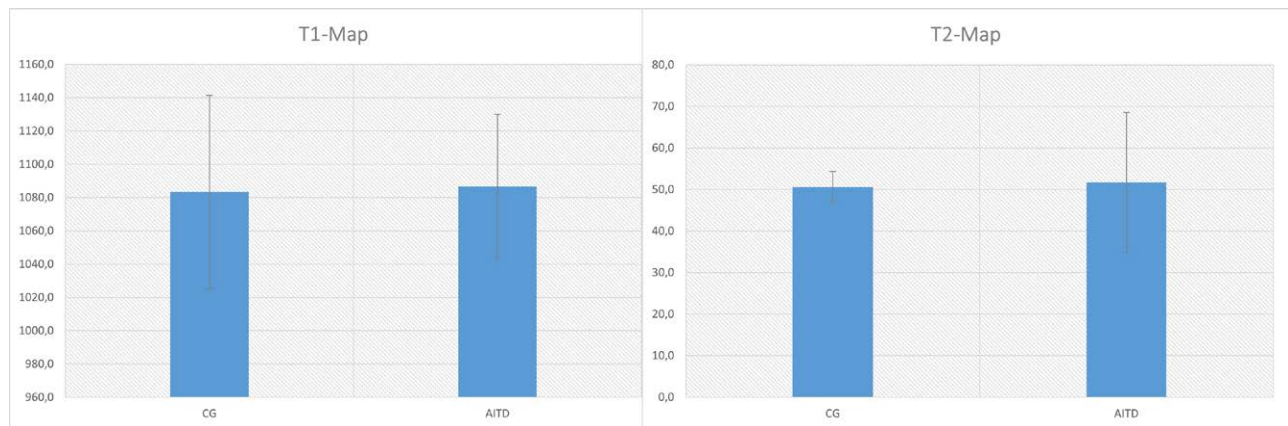Mapping sequences can provide additional information on different cardiac diseases such as myocardial infarction,

Figure 3. The diagram shows the distribution of the T1 and T2 mapping values and a comparison between the CG and AITD.
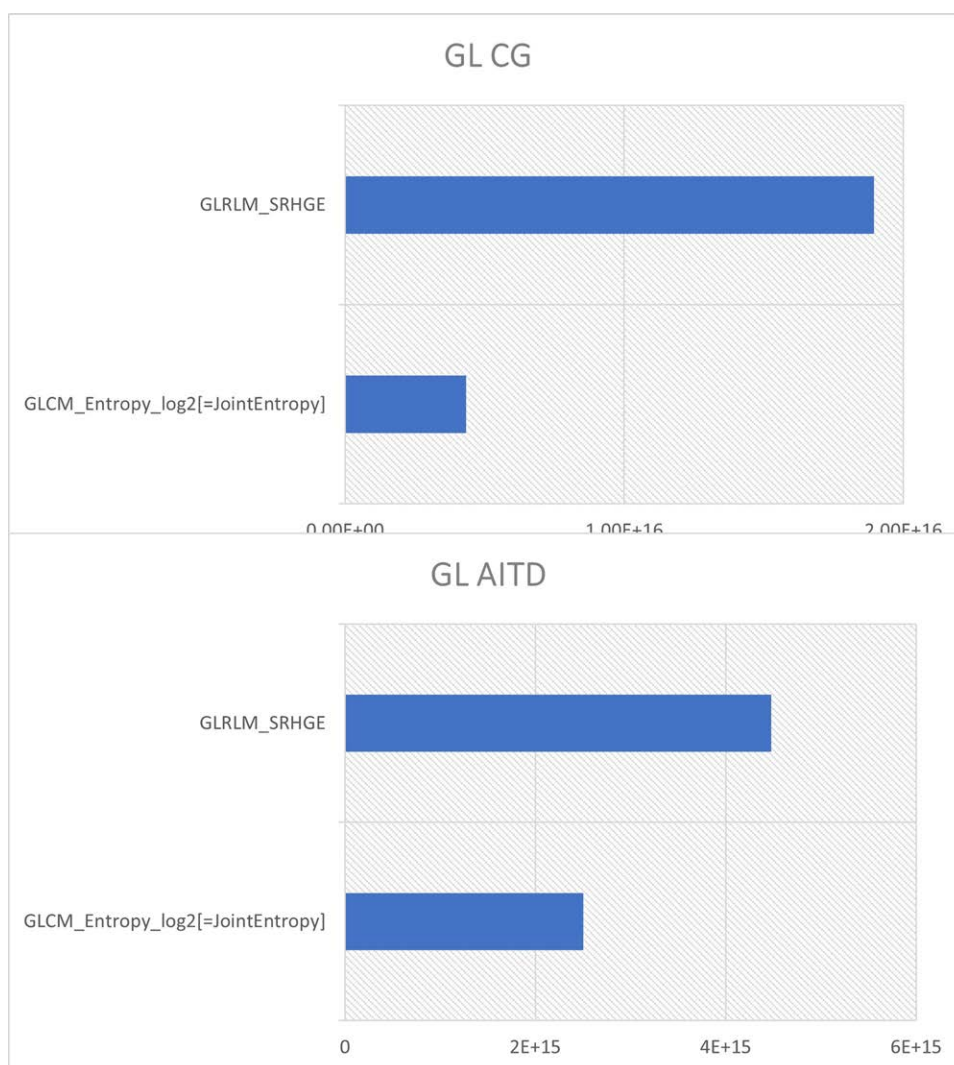

Figure 4. The diagram demonstrates the mean GL values between the CG and AITD.

myocarditis, hemochromatosis, fibrosis, Fabry disease, and amyloidosis. Furthermore, mapping sequences play an especially important role in the diagnosis of iron overload and the identification of focal myocardial edema and myocardial fibrosis. However, no cutoff values have been defined for the most common diseases. The only exception is the detection of iron overload, in which defined cutoff values are provided.

Using RC can lead to improved diagnostic accuracy.[23,24] In an RC analysis, Cetin et al evaluated the early impact of cardiovascular risk factors on the heart in patients with diabetes mellitus, high cholesterol, and high BP.[25] In Jang's found that only a small subset of RC properties was reproducible. In the FISP cine sequence, GLRLM was the most reproducible property.[26] In this study, we surveyed RC features on the hearts of patients with thyroid functional
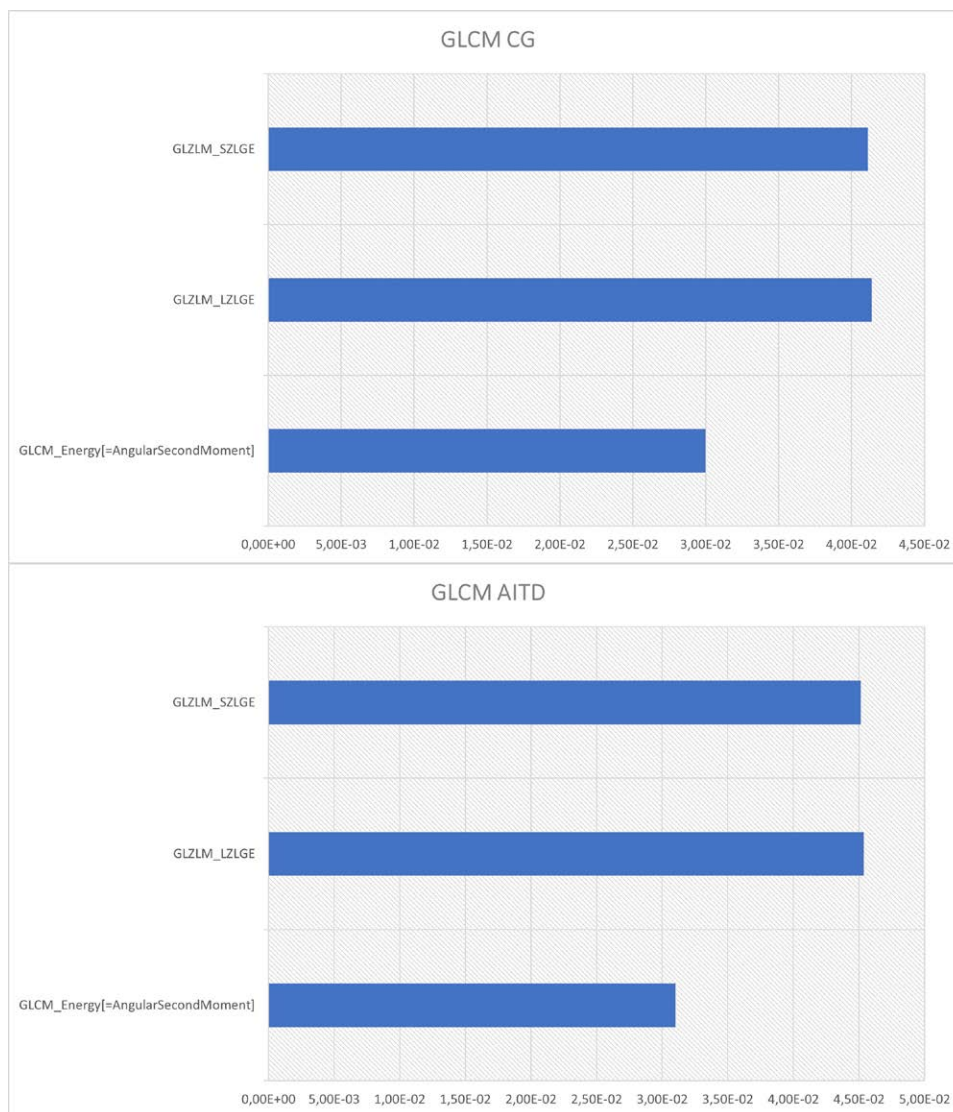
Figure 5. The mean GLCM values are shown in the diagram.

disorders and compared their results to those of the controls. Our data demonstrated a statistically significant difference in RC features and systolic and diastolic functions in patients with thyroid functional disorders compared to those in the CG. However, no significant changes were detected in cardiac mapping sequences.

In contrast to the study by Bengel et al, in which only CI and CO obtained by cardiac MRI were significantly altered in hyperthyroidism, we found significant differences in the RC features GLCM between patients with autoimmune thyroid disorder (AITD) and CG.[27]

Some confounding factors and knowledge gaps hinder the applicability of mapping techniques. Some of these are due to patient physiology, whereas others require scanner adjustments or field inhomogeneities.[28] Hence, no defined cutoff values are currently available for most diseases. In addition, many postprocessing methodologies have attempted to optimize diagnostic accuracy.[29,30] Mapping techniques can provide important additional information not found in standard CMR imaging; however, further studies on the standardization of data acquisition and postprocessing are needed.[28]

The information gained from the RC evaluation of CMR substantiates the significance of early diagnosis of cardiac changes in patients with AITD to prevent heart functional debasement with thyroid functional affection.

Our results demonstrate that single surveys utilizing CMR can be used to evaluate the impact of thyroid functional effects. In our study, RC and cardiac mapping were used secondary to laboratory, clinical, and echocardiographic parameters to approach the correct diagnosis.

5. Conclusion

Our study suggests that RC parameters extracted from CMR images can be used to discriminate between the AITD and CG groups. RC feature extraction and analysis of quantitative imaging parameters from CMR images may have a potential role in differentiating between patients in the AITD group and the CG. With the help of RC, CMR can potentially be a noninvasive technique that may play a major role in the identification of heart dysfunction.

Author contributions

The study design was overseen by the OB and SZ. Data acquisition was performed by MS and OB. Data analysis and interpretation were carried out by SZ and OB. A critical revision of the manuscript was performed by SM and KH. The study was supervised by SZ and KH.
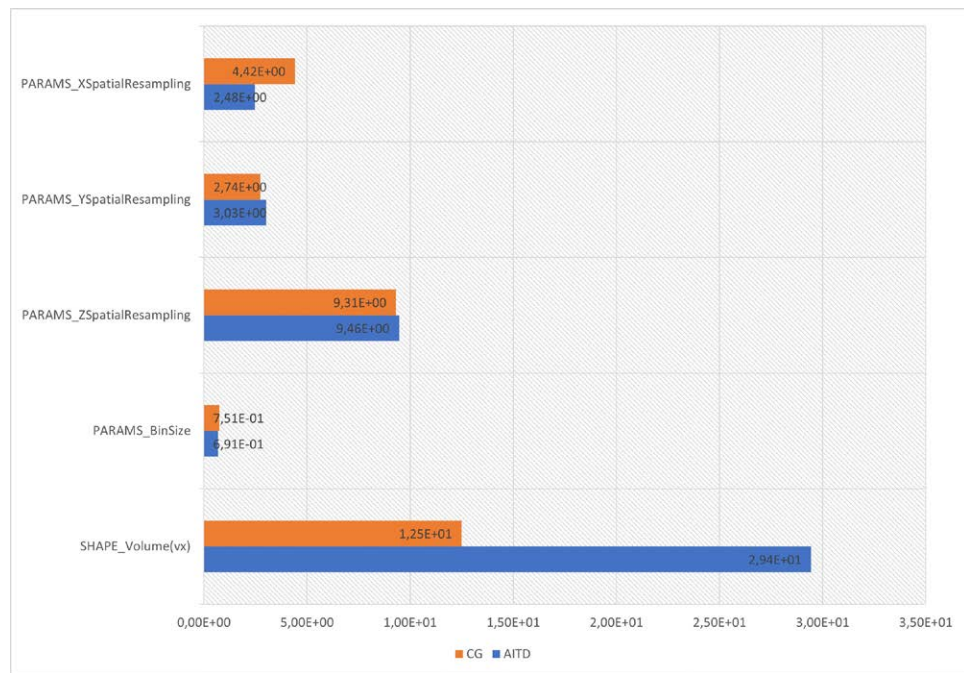
Figure 6. Diagram of the radiomics features' comparisons between the CG and AITD.

References

[1] Dayan CM, Daniels GH. Chronic autoimmune thyroiditis. N Eng J Med. 1996;335:99–107.

[2] Gencer B, Collet TH, Virgini V, et al. Subclinical thyroid dysfunction and the risk of heart failure events: an individual participant data analysis from 6 prospective cohorts. Circulation. 2012;126:1040–9.

[3] Biondi B. Mechanisms in endocrinology: heart failure and thyroid dysfunction. Eur J Endocrinol. 2012;167:609–18.

[4] Pearce EN, Yang Q, Benjamin EJ, et al. Thyroid function and left ventricular structure and function in the Framingham Heart Study. Thyroid. 2010;20:369–73.

[5] Zandieh S, Schuck L, Mirzaei S, et al. Evaluation of the cardiac morphologic alterations secondary to autoimmune thyroid disorder using cardiac magnetic resonance imaging. J Thorac Imaging. 2018;33:254–9.

[6] Kosar F, Sahin I, Aksoy Y, et al. Usefulness of pulsed-wave tissue doppler echocardiography for the assessment of the left and right ventricular function in patients with clinical hypothyroidism. Echocardiogr. 2006;23:471–7.

[7] Selmer C, Olesen JB, Hansen ML, et al. Subclinical and overt thyroid dysfunction and risk of all-cause mortality and cardiovascular events: a large population study. J Clin Endocrinol Metab. 2014;99:2372–82.

[8] Messroghli DR, Moon JC, Ferreira VM, , et al. Clinical recommendations for cardiovascular magnetic resonance mapping of T1, T2, T2* and extracellular volume: a consensus statement by the Society for Cardiovascular Magnetic Resonance (SCMR) endorsed by the European Association for Cardiovascular Imaging (EACVI). J Cardiovasc Magn Reson. 2017;19:75.

[9] Radenkovic D, Weingärtner S, Ricketts L, et al. Captur G T1 mapping in cardiac MRI. Heart Fail Rev. 2017;22:415–30.

[10] Aerts HJ, Velazquez ER, Leijenaar RT, et al. Decoding tumour phenotype by noninvasive imaging using a quantitative radiomics approach. Nat Commun. 2014;5:4006.

[11] Bahn RS, Burch HB, Cooper DS, et al. American thyroid association; american association of clinical endocrinolo- gists. hyperthyroidism and other causes of thyrotoxicosis: management guidelines of the american thyroid association and american association of clinical endocrinologists. Endocr Pract. 2011;17:456–520.

[12] Kawel-Boehm N, Maceira A, Valsangiacomo-Buechel ER, et al. Normal values for cardiovascular magnetic resonance in adults and children. J Cardiovasc Magn Reson. 2015;17:29.

[13] Plana JC, Galderisi M, Barac A, et al. Expert consensus report from the American society of echocardiography and the european association of cardiovascular imaging. Eur Heart J Cardiovasc Imaging. 2014;15:1063–93.

[14] Nioche C, Orlhac F, Boughdad S, et al. LIFEx: a freeware for radiomic feature calculation in multimodality imaging to accelerate advances in the characterization of tumor heterogeneity. Cancer Res. 2018;78:4786–9.

[15] Haralick RM, Shanmugam K, Dinstein I. Textural features for image classification. IEEE Trans Syst Man Cybern. 1973;3:610–21.

[16] Galloway MM. Texture classification using gray level run length. Comput Graph Image Process. 1975;4:172–9.

[17] Thibault G, Angulo J, Meyer F. Advanced statistical matrices for texture characterization: application to cell classification. IEEE Trans Biomed Eng. 2014;61:630–7.

[18] Mayerhoefer ME, Materka A, Langs G, et al. Introduction to radiomics. J Nucl Med. 2020;61:488–495.

[19] Biondi B, Palmieri EA, Lombardi G, et al. Subclinical hypothyroidism and cardiac function. Thyroid. 2002;12:505–10.

[20] Klein I, Ojamaa K. Thyroid hormone and the cardiovascular system. N Engl J Med. 2001;344:501–9.

[21] Danzi S, Klein I. Thyroid hormone and the cardiovascular system. Minerva Endocrinol. 2004;29:139–50.

[22] Baessler B, Luecke C, Lurz J, et al. Cardiac MRI texture analysis of T1 and T2 maps in patients with infarctlike acute myocarditis. Radiology. 2018;289:357–65.

[23] Ponsiglione A, Stanzione A, Cuocolo R, et al. Cardiac CT and MRI radiomics: systematic review of the literature and radiomics quality score assessment. Eur Radiol. 2022;32:2629–38.

[24] Gao Z, Wang X, Sun S, et al. Learning physical properties in complex visual scenes: an intelligent machine for perceiving blood flow dynamics from static CT angiography imaging. Neural Netw. 2020;123:82–93.

[25] Cetin I, Raisi-Estabragh Z, Petersen SE, et al. Radiomics signatures of cardiovascular risk factors in cardiac MRI: results from the UK biobank. Front Cardiovasc Med. 2020;7:591368.

[26] Jang J, Ngo LH, Mancio J, et al. Reproducibility of segmentation-based myocardial radiomic features with cardiac MRI. Radiol Cardiothorac Imaging. 2020;2:e190216.

[27] Bengel FM, Nekolla SG, Ibrahim T, et al. Effect of thyroid hormones on cardiac function, geometry, and oxidative metabolism assessed noninvasively by positron emission tomography and magnetic resonance imaging. J Clin Endocrinol Metab. 2000;85:1822–7.

[28] Messroghli DR, Moon JC, Ferreira VM, et al. Clinical recommendations for cardiovascular magnetic resonance mapping of T1, T2, T2* and extracellular volume: a consensus statement by the Society

for Cardiovascular Magnetic Resonance (SCMR) endorsed by the European Association for Cardiovascular Imaging (EACVI). J Cardiovasc Magn Reson. 2017;19:75.

[29] Shao J, Rapacchi S, et al. Myocardial T1 mapping at 3.0 tesla using an inversion recovery spoiled gradient echo readout and Bloch equation simulation with slice profile correction (BLESSPC) T1 estimation algorithm. Magn Reson Imaging. 2016;43:414–25.

[30] Shao J, Nguyen K-L, et al. J Instantaneous signal loss simulation (InSiL): an improved algorithm for myocardial T1 mapping using the MOLLI sequence. J Magn Reson Imaging. 2015;41:721–9.